

Gray algebraic curve model-based roof separation prediction method for the warning of roof fall accidents

Jian-Lin Xie¹ · Jia-Lin Xu^{1,2} · Wei-Bing Zhu²

Received: 19 March 2014 / Accepted: 3 June 2016 / Published online: 14 June 2016
© Saudi Society for Geosciences 2016

Abstract Roof separation is one of the main precursors of coal mine accidents at the workplace. At present, indicator data are usually read in an attempt to understand the real-time changes of the roof separation, but the change trend cannot be predicted. Predicting the change trend of roof separation on time can play a very important role in roof control. In this study, we apply the gray theoretical analysis method to predict the change trend of roof separation. We use Universal Distinct Element Code (UDEC) numerical simulation software to simulate the generation processes of roof separation. For this purpose, we consider four scenarios with different immediate roof heights. Using experimental separation data as original data, we predict roof separation using the gray algebraic curve model (GAM). The GAM-predicted data show little error when compared with the experimental data and are also better compared with prediction data obtained with the traditional gray model GM(1,1). Finally, in a case study using field-monitoring roof separation data from a mine, the GAM method led to good prediction results, and the predicted development trend reflected the real conditions. Thus, we prove that GAM is a very effective prediction method, which will be very useful in predicting roof separation trends for the warning of roof fall accidents.

Keywords Gray algebraic curve model · Roof fall accident warning · Roof separation · Change trend prediction

Introduction

Roof fall accidents currently account for about 40 % of all coal mine accidents (shown in Table 1), ranking first among those in China. In recent years, roof fall accidents at the coal mine workplace have significantly declined, due to improvements in the fully mechanized coal-mining equipment, the development of supporting technology, and especially the promotion of a comprehensive workplace support quality-monitoring system. Consequently, the number of deaths caused by roof fall accidents has been effectively controlled and reduced lately. However, roof fall accidents continue to significantly contribute to a growing annual number of coal mine accidents. According to incomplete statistics, the number of deaths from roof fall accidents accounts for 50 % of the deaths from all accidents in small coal mines in a number of counties and townships in China. Therefore, a further study of technologies aiming at prevention of roof fall accidents must be undertaken to assure coal mine safety in the future.

Many scholars had done a lot of researches in the analysis of roof separation for roof control. Ling et al. (2003) comprehensively investigated the condition of the rock medium, environmental occurrence conditions, and engineering factors. In addition, they established a dynamic model for predicting the roof stability of mining fields using artificial neural network tool. Tan et al. (2006) proposed that the occurrence of peaks in the roof separation velocity was applicable for forecasting the falling of inferior roofs. In addition, they developed a roof separation telemetering system for measuring and forecasting roof falls. Zhang et al. (2010) gave the necessity conditions of load, span, and deflection, which were

✉ Jia-Lin Xu
34884208@qq.com

¹ State Key Laboratory of Coal Resources and Safe Mining, China University of Mining and Technology, Xuzhou, Jiangsu 221116, People's Republic of China
² School of Mining Engineering, China University of Mining and Technology, Xuzhou, Jiangsu 221116, People's Republic of China

Table 1 The statistical analysis of coal mine accidents in China

Different causes of accidents	Roof fall	Gas	Transportation	Water inrush	Fire	Blasting	Mechanical and electrical	Other causes
The proportion of accident number	47 %	9.2 %	18.6 %	3.1 %	0.6 %	3.1 %	7.2 %	11.2 %
The proportion of death number	33.2 %	25.3 %	14.5 %	8.8 %	1.9 %	1.8 %	4.2 %	10.3 %

The data in the table cited from statistical analysis of China coal mine accidents in 2012 by Xu et al. (2015)

proposed for roof separation in the immediate roof. Tang et al. (2010) analyzed the relationship between the roof separation and the roof deformation under the support method of combined support with anchor. Bertoncini and Hinders (2010) made fuzzy classification of roof fall predictors in microseismic monitoring. Saeedi et al. (2013) presented the effect of exposed area geometry on potential roof falls using the 2D numerical modeling program. A novel fuzzy inference system has been made for predicting roof fall rate in underground coal mines (Razani et al. 2013; Farid et al. 2013; Ghasemi and Ataei 2013). Yan et al. (2014) studied the influencing factors of the roof separation of the roadway with extra-thick coal seam. The underground roadway roof separation was monitored in time by fiber Bragg grating sensors (Zhao et al. 2015). Salient findings of field instrumentation data analysis such as mining-induced vertical stress development over the pillars, load over the support, roof separation at different horizons, and convergence of roof in rooms with face advance were presented (Satyanarayana et al. 2015). Khan et al. (2015) use wireless sensor networks to determine cluster breakage by sudden disruptions caused by roof falls. Xie and Xu (2015) took ground-penetrating radar (GPR) as a means for roof separation detection and analyzed its feasibility for use in detecting roof separation both theoretically and experimentally.

In the performance evaluation of roadway support, roof separation has always been a major index. When roof separation exceeds a certain critical value, the roof is regarded as unstable. Under these conditions, unless timely support measures are taken, a roof fall accident is likely to occur. At present, understanding the real-time changes of the roof separation is mainly achieved by reading the indicator data, but the

change trend cannot be predicted. Finding a way to predict the change trend of roof separation will play a very important role in roof control.

Roof separation is induced by multiple geological factors and complex mechanical behaviors that are not yet fully understood. To effectively predict and control roof fall accidents, a clear understanding of the characteristic variations of roof separation is necessary. However, it is not yet clear how to use mathematical models to predict roof separation. Moreover, predicting this complex process is very difficult, due to the many parameters involved. According to the gray system theory proposed by Deng (1987), an irregular information sequence in an arbitrary stochastic process may be transformed into a regular information sequence by generating the transformation. When using this theory, there is no need to know the distribution characteristics of the original data in the mathematical model. Moreover, for a small number of discrete data sequences, the modeling requirements can be met simply by generating the transformation several times. Furthermore, the prediction results from the application of this model are more accurate and more consistent with the real conditions, compared with other prediction models.

The gray model has not been used before to predict the change trend of roof separation, so that this article is the first to attempt such a prediction. When using a gray theoretical analysis, only a small amount of existing roof separation data is required to predict the development trend of roof separation. The results obtained can then provide auxiliary decision-making information for predicting roof fall accidents.

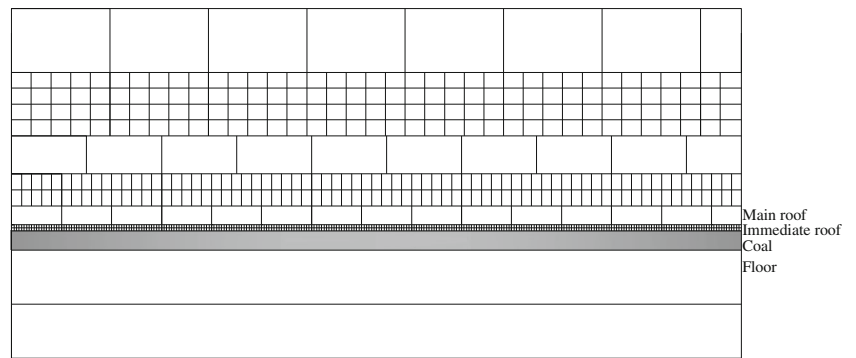
Gray algebraic curve model-based prediction method

The gray system primarily includes system modeling, model testing, correlation analysis, clustering evaluation, decision making, and planning. The gray system theory is used to reduce the uncertainty resulting from random factors, thus increasing the objective regularity of a system through the mathematical processing of the original system information sequences. The system is then modeled using corresponding mathematical differential equations (Liu 1999). The discrete time series generated by the original sequence accumulation is transformed into a differential equation that is continuous in

Table 2 Precision inspection grading table

Precision grade	Criticality of index		
	Relative error Δ (%)	Ratio of mean square ratio C	Possibility of small error P
Grade 1 (good)	1	0.35	0.95
Grade 2 (qualified)	5	0.50	0.80
Grade 3 (reluctantly qualified)	10	0.65	0.70
Grade 4 (disqualified)	20	0.80	0.60

Fig. 1 Simulation model



time. The resulting function model is known as the gray model (GM).

The exponential solutions of the GM model differential equation have been used to determine that the GM prediction method is only applicable to conditions, in which the original sequence shows exponential variations. The gray prediction refers to the generation of cumulative sequence by using an exponential function to simulate the original random sequence. However, the cumulative generation sequence may not vary exponentially. Therefore, the GM model is limited in its capability to analyze complex and nonlinear problems and thus cannot be used to effectively simulate and predict a nonlinear system. For an arbitrary deterministic system, prediction can be approached by using a polynomial function. Thus, the cumulative generation sequence reduces the degree of randomness and enhances the regularity of the original sequence. Meanwhile, by combining this sequence with the polynomial function, it functions intensively in the approach of discrete data and in turn develops into a gray algebraic curve model (GAM) that can more effectively simulate and predict the solutions of nonlinear problems (Qi et al. 2004; Ou et al. 2005; Wang 2012).

We assume here that the original data sequence observed is $X^{(0)} = (X^{(0)}(1), X^{(0)}(2), \dots, X^{(0)}(n))$, which develops into $X^{(1)} = (X^{(1)}(1), X^{(1)}(2), \dots, X^{(1)}(n))$ after one accumulation.

$$X^{(1)}(i) = \sum_{j=1}^i X^{(0)}(j), i = 1, 2 \dots n \tag{1}$$

We then hypothesize that $X^{(1)}$ is the algebraic curve on sequence k . The GAM of $X^{(1)}$ is then

$$\hat{X}^{(1)}(k) = a_0 + a_1k + a_2k^2 + \dots + a_mk^m = \sum_{i=0}^m a_i k^i \tag{2}$$

In Eq. (2), the coefficients a_0, a_1, \dots, a_m are undetermined parameters, and $k = 1, 2, \dots, n$.

Let

$$A = [a_0, a_1, \dots, a_m]^T \tag{3}$$

$$Y = \begin{bmatrix} X^{(1)}(1) \\ X^{(1)}(2) \\ \vdots \\ X^{(1)}(n) \end{bmatrix} \tag{4}$$

$$B = \begin{bmatrix} 1 & 1 & \dots & 1^m \\ 1 & 2 & \dots & 2^m \\ 1 & 3 & \dots & 3^m \\ \vdots & \vdots & \ddots & \vdots \\ 1 & n & \dots & n^m \end{bmatrix} \tag{5}$$

Table 3 Parameters of each rock stratum in the model

Stratum no.	Lithology	Thickness (m)	Bulk modulus (GPa)	Shear modulus (GPa)	Unit weight (kN/m ³)	Internal friction angle (deg)	Tensile strength (MPa)	Cohesion (MPa)
1	Sandstone	10	15	8.5	25.0	32	3.5	5.0
2	Mudstone	10	8	5.0	23.0	25	1.0	2.5
3	Sandstone	6	15	8.5	25.0	32	3.5	5.0
4	Mudstone	5	8	5.0	23.0	25	1.0	2.5
5	Sandstone (main roof)	3	15	8.5	25.0	32	3.5	5.0
6	Mudstone (immediate roof)	1	8	5.0	23.0	25	1.0	2.5
7	Coal	3	6	4.5	13.0	20	0.6	2.0
8	Granite (floor)	17	20	12.0	27.0	35	5.0	9.0

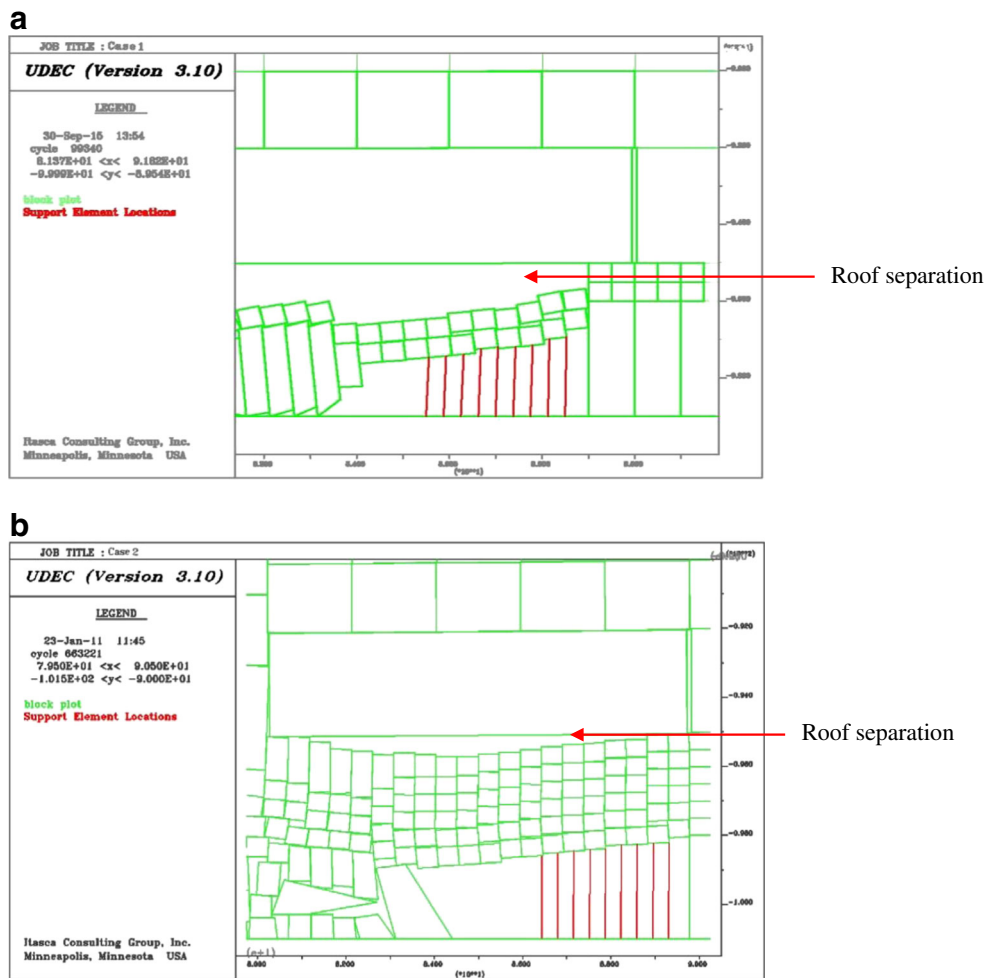


Fig. 2 State of roof separation in the four simulation models. **a** State of roof separation in the simulation model of case 1. **b** State of roof separation in the simulation model of case 2. **c** State of roof separation in the simulation model of case 3. **d** State of roof separation in the simulation model of case 4

The residual vector $E = (Y - BA)$. If $E^2 = (Y - BA)^2 \rightarrow \min$, which yields Eq. (6) by the least squares method,

$$A = (B^T B)^{-1} B^T Y \tag{6}$$

Substituting the coefficients in Eq. (6) in the GAM equation, we obtain the cumulative generating sequence. After a one-time regressive reduction, the prediction data are obtained as

$$\hat{X}^{(0)}(k) = \hat{X}^{(1)}(k) - \hat{X}^{(1)}(k-1) \tag{7}$$

To summarize, the GAM proceeds as follows:

- (1) Calculate the one-time cumulative generating sequence $X^{(1)}$ according to the original data sequence $X^{(0)}$;
- (2) Determine the maximum times m of the optimal curve;
- (3) Establish the B and Y matrices;
- (4) Calculate the uncertainty coefficients a_i according to $A = (B^T B)^{-1} B^T Y$;

- (5) Establish the prediction model;
- (6) Obtain the prediction sequence $\hat{X}^{(0)}$; and
- (7) Determine the accuracy of the model.

The accuracy of the simulated data obtained from above should be determined to investigate the goodness of fit of the prediction model. The original sequence is assumed to be $X^{(0)} = (X^{(0)}(1), X^{(0)}(2), \dots, X^{(0)}(n))$, and the corresponding simulated sequence is $\hat{X}^{(0)} = (\hat{X}^{(0)}(1), \hat{X}^{(0)}(2), \dots, \hat{X}^{(0)}(n))$.

The mean of the original sequence $X^{(0)}$ is

$$\bar{X} = \frac{1}{n} \sum_{k=1}^n X^{(0)}(k) \tag{8}$$

The variance of the original sequence $X^{(0)}$ is

$$s_1^2 = \frac{1}{n} \sum_{k=1}^n (X^{(0)}(k) - \bar{X})^2 \tag{9}$$

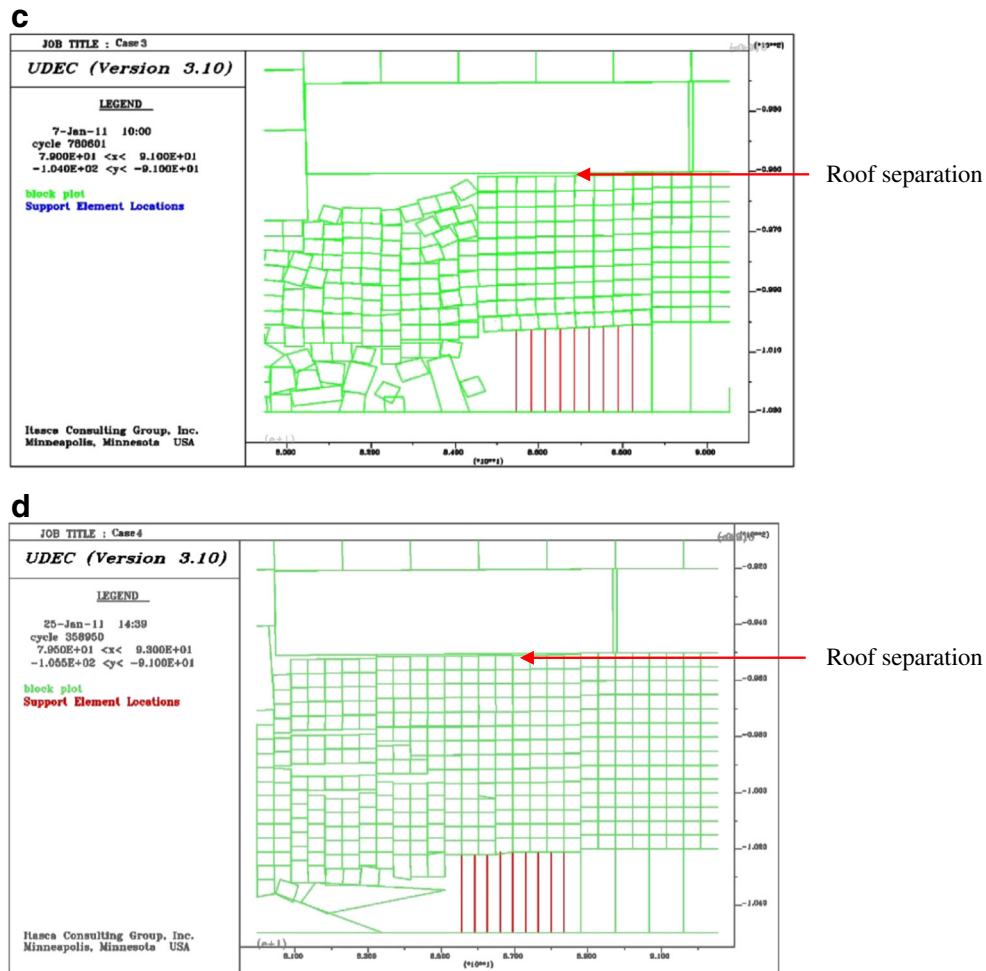


Fig. 2 (continue)

The residual sequence from the original and simulated sequences is

$$\varepsilon^{(0)} = \{\varepsilon(1), \varepsilon(2), \dots, \varepsilon(n)\} \\ = \left\{ X^{(0)}(1) - \hat{X}^{(0)}(1), X^{(0)}(2) - \hat{X}^{(0)}(2), \dots, X^{(0)}(n) - \hat{X}^{(0)}(n) \right\} \quad (10)$$

The mean of the residual is

$$\bar{\varepsilon} = \frac{1}{n} \sum_{k=1}^n \varepsilon(k) \quad (11)$$

Table 4 Roof separation data of the four simulation cases

Original no.	1	2	3	4	5	6
The data of case 1 (mm)	5.2	14.05	57.2	130.5	181.8	300.6
The data of case 2 (mm)	2.18	18.01	56.69	87.08	174.22	232.48
The data of case 3 (mm)	2.04	8.95	20.25	67.79	160.96	229.29
The data of case 4 (mm)	1.00	4.75	8.09	18.62	35.53	46.83

The variance of the residual is

$$s_2^2 = \frac{1}{n} \sum_{k=1}^n (\varepsilon(k) - \bar{\varepsilon})^2 \quad (12)$$

The relative error sequence from the original and simulation sequences is

$$\Delta = \left\{ \left| \frac{\varepsilon(1)}{X^{(0)}(1)} \right|, \left| \frac{\varepsilon(2)}{X^{(0)}(2)} \right|, \dots, \left| \frac{\varepsilon(n)}{X^{(0)}(n)} \right| \right\} = \{\Delta_k|_1^n\} \quad (13)$$

The ratio of the mean square error is

$$C = \frac{s_2}{s_1} \quad (14)$$

The probability of a small error is

$$P = P(|\varepsilon(k) - \bar{\varepsilon}| < 0.6745s_1) \quad (15)$$

Table 2 shows the precision inspection grade of the prediction model.

Table 5 Lagrange interpolation results from the experimental data of roof separation and the results from the four simulation cases

No. after interpolation	1	2	3	4	5	6	7	8	9
The data of case 1 after interpolation (mm)	5.2	14.05	32.02 ^a	57.2	90.49 ^a	130.5	181.8	236.75 ^a	300.6
The data of case 2 after interpolation (mm)	2.18	7.78 ^a	18.01	33.98 ^a	56.69	87.08	125.99 ^a	174.22	232.48
The data of case 3 after interpolation (mm)	2.04	3.50 ^a	8.95	20.25	39.24 ^a	67.79	107.74 ^a	160.96	229.29
The data of case 4 after interpolation (mm)	1.00	2.45 ^a	4.75	8.09	12.65 ^a	18.62	26.18 ^a	35.53	46.83

^a The data are obtained after interpolation

Numerical simulations

To simulate the separation development in a composite roof, we use a discrete element numerical simulation software, Universal Distinct Element Code (UDEC). Figure 1 shows the two-dimensional numerical calculation model of case 1. This model is 150 m long and 55 m high. The horizontal coal seam therein is 3 m thick. The immediate roof is 1 m thick, and the blocks of the immediate roof are further divided into blocks of 0.5 × 0.5-m² size. The main roof is 3 m thick, and the main roof is divided into blocks of 10 × 3 m². The boundary of the model is fixed by displacement, and the model obeys the Mohr–Coulomb constitutive relationship. Table 3 shows the lithology, thickness, and mechanical parameters of the main rock strata in the model.

To explore the influence of different values of the immediate roof thicknesses on roof separation, three additional model cases are added to the model above. The immediate roof thickness in cases 2 to 4 are set at 3, 5, and 7 m, respectively, while the other parameters are the same as those in case 1.

The model coal mine was excavated in the following two steps in the simulation:

Step 1: Initial balancing of the model; and

Step 2: Excavation of the coal mine at a pace of 1.0 m at each step of the simulation, from left to right, while the roof is supported by pillars.

The three additional model cases were simulated following the two steps listed above. Figure 2 shows the roof separation produced by the simulations for each case.

Table 4 lists the roof separation data obtained by roof separation observations at the workface of the four model cases in the numerical simulations and by recording the variations in the roof separation from generation to gradual expansion.

GAM prediction results and discussion

Table 5 presents Lagrange interpolation results of the experimental data from Table 4.

The cumulative sequence of the first seven data in Table 4 was calculated using Eq. (1). According to Eq. (4), we determined that

$$\begin{aligned}
 Y_1 &= [5.20 \ 19.25 \ 51.27 \ 108.47 \ 198.96 \ 329.46 \ 511.26]^T \\
 Y_2 &= [2.18 \ 9.96 \ 27.97 \ 61.95 \ 118.64 \ 205.72 \ 331.71]^T \\
 Y_3 &= [2.04 \ 5.54 \ 14.49 \ 34.74 \ 73.98 \ 141.77 \ 249.51]^T \\
 Y_4 &= [1.00 \ 3.45 \ 8.20 \ 16.29 \ 28.94 \ 47.56 \ 73.74]^T
 \end{aligned}$$

Table 6 GAM-predicted data, residuals, and relative errors of the roof separation in case 1

No. after interpolation	Original sequence (mm)	Predicted sequence (mm)	Residual (mm)	Relative error (%)
1	5.2	5.0506	0.1494	2.87
2	14.05	14.5087	-0.4587	-3.26
3	32.02	31.7351	0.2849	0.89
4	57.2	56.9883	0.2117	0.37
5	90.49	90.2682	0.2218	0.25
6	130.5	131.575	-1.075	-0.82
7	181.8	180.9085	0.8915	0.49

Table 7 GAM-predicted data, residuals, and relative errors of the roof separation in case 2

No. after interpolation	Original sequence (mm)	Predicted sequence (mm)	Residual (mm)	Relative error (%)
1	2.18	1.979	0.201	9.22
2	7.78	8.452	-0.672	-8.64
3	18.01	17.463	0.647	3.59
4	33.98	33.656	0.324	0.95
5	56.69	57.031	-0.341	-0.60
6	87.08	87.592	-0.512	-0.59
7	125.99	125.333	0.657	0.52

Table 8 GAM-predicted data, residuals, and relative errors of the roof separation in case 3

No. after interpolation	Original sequence (mm)	Predicted sequence (mm)	Residual (mm)	Relative error (%)
1	2.04	2.243	-0.203	-9.95
2	3.50	3.423	0.077	2.2
3	8.95	8.490	0.450	5.03
4	20.25	20.182	0.068	0.34
5	39.24	40.492	-1.252	-3.19
6	67.79	69.445	-1.655	-2.44
7	107.74	107.004	0.736	0.68

Table 9 GAM-predicted data, residuals, and relative errors of the roof separation in case 4

No. after interpolation	Original sequence (mm)	Predicted sequence (mm)	Residual (mm)	Relative error (%)
1	1.00	0.96	0.04	4.0
2	2.45	2.582	-0.132	-12.24
3	4.75	4.643	0.107	2.25
4	8.09	8.021	0.069	0.85
5	12.65	12.713	-0.063	-0.49
6	18.62	18.719	-0.099	-0.53
7	26.18	26.041	0.139	0.53

By comparison, we determined that the fitting is optimal for a maximum time of $m = 3$. Using Eqs. (3)–(6), we find that

$$B = \begin{bmatrix} 1 & 1 & 1 & 1 \\ 1 & 2 & 4 & 8 \\ 1 & 3 & 9 & 27 \\ 1 & 4 & 16 & 64 \\ 1 & 5 & 25 & 125 \\ 1 & 6 & 36 & 216 \\ 1 & 7 & 49 & 343 \end{bmatrix}$$

$$A_1 = \begin{bmatrix} -0.2586 \\ 3.3850 \\ 0.5863 \\ 1.3378 \end{bmatrix}$$

$$A_2 = \begin{bmatrix} -4.6471 \\ 8.1073 \\ -2.6783 \\ 1.1972 \end{bmatrix}$$

$$A_3 = \begin{bmatrix} -8.7371 \\ 16.6332 \\ -7.0907 \\ 1.4374 \end{bmatrix}$$

$$A_4 = \begin{bmatrix} -0.8728 \\ 1.8974 \\ -0.2833 \\ 0.2191 \end{bmatrix}$$

Using Eq. (2), we obtain the following corresponding gray curve model equations:

$$\hat{X}_1^{(1)}(k) = -0.2586 + 3.385k + 0.5863k^2 + 1.3378k^3$$

$$\hat{X}_2^{(1)}(k) = -4.6471 + 8.1073k - 2.6783k^2 + 1.1972k^3$$

$$\hat{X}_3^{(1)}(k) = -8.7371 + 16.6332k - 7.0907k^2 + 1.4374k^3$$

$$\hat{X}_4^{(1)}(k) = -0.8728 + 1.8974k - 0.2833k^2 + 0.2191k^3$$

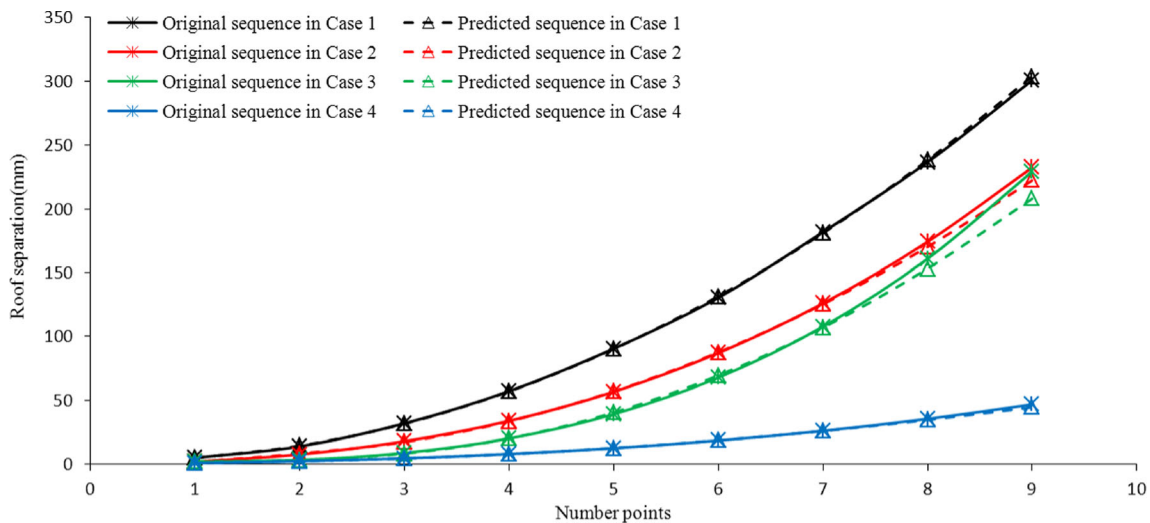


Fig. 3 GAM-predicted and original curves for the experimental data

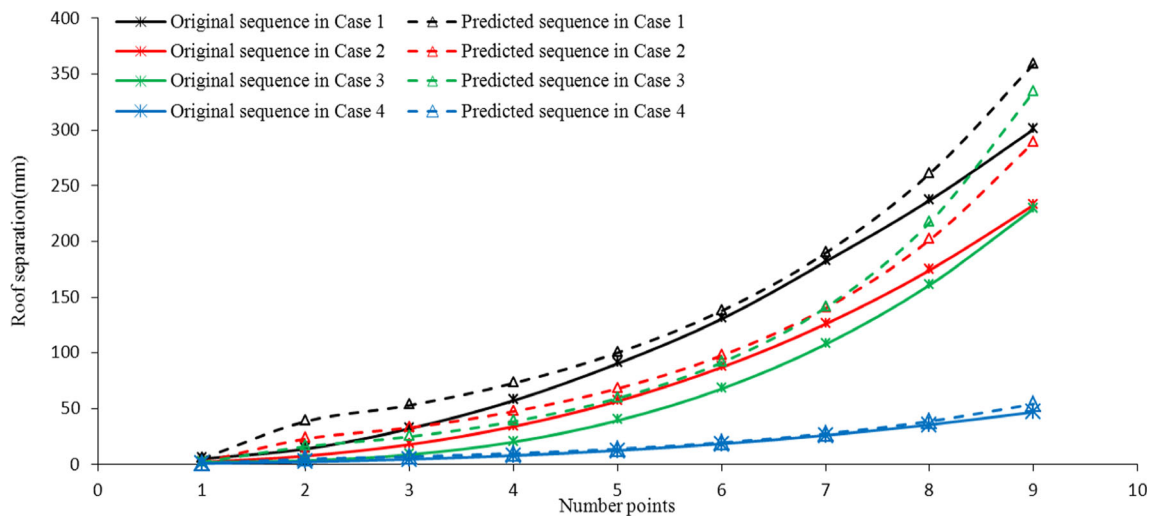


Fig. 4 GM(1,1)-predicted and original curves for the experimental data

Substituting for the number k (from 1 to 7) into the formulas above, the k represents the time point which is equivalent to the time as $k\Delta t$, according to the actual situation; here, Δt can be several days or hours, etc. The predicted sequence, the residual, and the relative error can be solved by Eqs. (7), (10), and (13), respectively, as shown in Tables 5, 6, 7, and 8.

The values for $k = 8$ and $k = 9$ are predicted to be 238.269 and 303.656 mm, respectively, in case 1. In Table 4, the two time points of case 1 are experimentally set at 236.75 and 300.60 mm, respectively. The residuals of the predicted data compared with the experimental data of the two time points are -1.52 and -3.01 mm, while the relative errors are -0.64 and -1.02 %, respectively. Error detection in the predicted data in Table 6 shows that the mean square deviation ratio solved by Eq. (14) is $C = 0.01 < 0.35$, while the small error probability solved by Eq. (15) is $P = 1$.

The values for $k = 8$ and $k = 9$ are predicted to be 170.260 and 222.369 mm, respectively, in case 2. In Table 4, the two time points of case 2 are experimentally set at 174.22 and 232.48 mm,

respectively. The residuals of the predicted data from the experimental data of the two time points are 3.96 and 10.11 mm, while the relative errors are 2.3 and 4.3 %, respectively. Error detection in the predicted data in Table 7 shows that the mean square deviation ratio solved by Eq. (14) is $C = 0.03 < 0.35$, while the small error probability solved by Eq. (15) is $P = 1$.

The values for $k = 8$ and $k = 9$ are predicted to be 153.193 and 208.007 mm, respectively, in case 3. In Table 4, the two time points of case 3 are experimentally set as 160.96 and 229.29 mm, respectively. The residuals of the predicted data with the experimental data of the two time points are 7.77 and 21.28 mm, while the relative errors are 4.8 and 9.3 %, respectively. Error detection in the predicted data in Table 8 shows that the mean square deviation ratio solved by Eq. (14) is $C = 0.05 < 0.35$, while the small error possibility solved by Eq. (15) is $P = 1$.

The values for $k = 8$ and $k = 9$ are predicted to be 34.675 and 44.626 mm, respectively, in case 4. In Table 4, the two time points of case 4 are experimentally set as 35.53 and 46.83 mm, respectively. The residuals of the predicted data with the experimental data of the two time points are 0.86 and 2.20 mm, while the relative errors are 2.4 and 4.7 %,

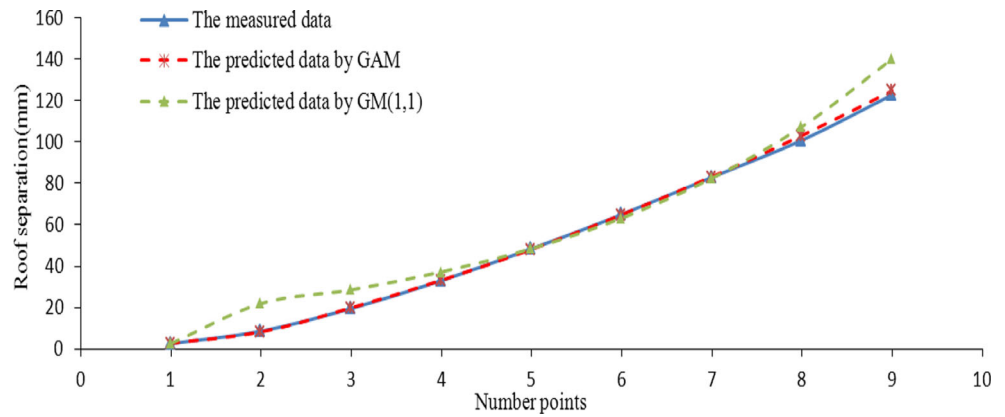


Fig. 5 Roof separation field-monitoring diagram

Table 10 GAM-predicted data, residuals, and relative errors of the roof separation from the field measurements

No.	Measured sequence (mm)	Predicted sequence (mm)	Residual (mm)	Relative error (%)
1	2.5	2.607	-0.107	-4.29
2	8.5	8.131	0.369	4.34
3	19.5	19.822	-0.322	-1.65
4	33	33.180	-0.180	-0.54
5	48.5	48.204	0.296	0.61
6	65	64.895	0.105	0.16
7	83	83.253	-0.253	-0.31

Fig. 6 GAM- and GM(1,1)-predicted and original curves for the field measurements



respectively. Error detection in the predicted data in Table 9 shows that the mean square deviation ratio solved by Eq. (14) is $C = 0.09 < 0.35$, while the small error possibility solved by Eq. (7) is $P = 1$.

By observing the errors in Tables 5, 6, 7, and 8 and referring to the precision detection grade control in Table 1, we find that most of the GAM prediction results are within precision grade 1. Figure 3 shows the curves from the GAM predictions and the experimental data of roof separation in Tables 5, 6, 7, and 8. As shown in Fig. 3, it is clear that the GAM prediction data show little error with respect to the experimental data. Moreover, the prediction trend reflects the experimental results. For comparison, when the traditional gray model GM(1,1) is used to forecast the experimental data, most of the predicted results do not meet the necessary requirements (Fig. 4). Thus, we prove that the GAM approach is more effective in predicting roof separation trends than GM(1,1).

A case study

As an example, the Qidong coal mine in the Anhui Province of China makes use of a mechanical displacement meter to monitor the roadway roof separation. The shallow and deep basis points of the displacement meter were set at 3 and 6 m, respectively, above the roof interface (Fig. 5).

By selecting the first seven data from field measurement, and using the GAM method, we obtain the corresponding gray curve model equation as follows:

$$\hat{X}^{(1)}(k) = 4.5000 - 6.3492k + 4.1786k^2 + 0.2778k^3 \quad (16)$$

Substituting k with 1 to 7 into the formulas above, we can solve the predicted sequence, residual, and relative error with Eqs. (7), (10), and (13), as shown in Table 9.

The values for $k = 8$ and $k = 9$ are predicted to be 103.278 and 124.970 mm, respectively. The two time points of field measurement data were 101 and 123 mm, respectively. The residuals of the predicted data compared with the

experimental data of the two time points are -2.28 and -1.97 mm, while the relative errors are -2.3 and -1.6 %, respectively. Error detection in the predicted data in Table 10 shows that the mean square deviation ratio solved by Eq. (14) is $C = 0.03 < 0.35$, while the small error probability solved by Eq. (7) is found to be $P = 1$, and the prediction level is grade 1. Figure 6 shows the curves corresponding to the GAM and GM(1,1) predictions and the field measurements.

Conclusions

- (1) We introduce the GAM modeling approach and apply it for the first time to forecast the change trend of roof separation.
- (2) To build our prediction model based on the GAM method, we use the roof separation data from a UDEC numerical simulation as the original observation data. We then apply the prediction model to predict the development trends of roof separation. The prediction data show little error with respect to the experimental data, and the trend is consistent with the experimental observations. For the sake of comparison, we also apply the traditional GM(1, 1) method and find that the predicted error was larger than that in the GAM application. Thus, we prove that GAM is the more effective method for predicting roof separation trends.
- (3) In the case study making use of field-monitoring roof separation data from a mine, the GAM method leads to good prediction results. When we get the warning criterion of roof separation of a roadway according to empirical data statistical analysis, and set roof separation indicators to get a small amount data, then, we can predict the development trend of roof separation using GAM method based on the existing data. The GAM method provides the desired auxiliary decision-making information that can be used to issue warnings about roof fall accidents and thus has the greatest potential to help reduce and avoid these accidents.

Acknowledgments This work has been supported by the Fundamental Research Funds for the Central Universities (No. 2015QNB15) and the project funded by the Priority Academic Program Development of Jiangsu Higher Education Institutions (SZBF2011-6-B35).

References

- Bertoncini CA, Hinders MK (2010) Fuzzy classification of roof fall predictors in microseismic monitoring. *Measurement* 43:1690–1701
- Deng JL (1987) Gray system method. Huazhong University of Science and Technology Press, Wuhan, pp. 110–118 (in Chinese)
- Farid M, Hossein Abadi MM, Yazdani-Chamzini A, et al. (2013) Developing a new model based on neuro-fuzzy system for predicting roof fall in coal mines. *Neural Comput & Applic* 23: 129–137
- Ghasemi E, Ataei M (2013) Application of fuzzy logic for predicting roof fall rate in coal mines. *Neural Comput & Applic* 22:311–321
- Khan MY, Qaisar SB, Naeem M, et al. (2015) Detection and self-healing of cluster breakages in mines and tunnels: an empirical investigation. *Sens Rev* 35:263–273
- Ling BC, Peng SP, Meng ZP (2003) The dynamic prediction and control on the roof stability of stope. *J Eng Geol* 11:44–48 (in Chinese)
- Liu SF (1999) Gray system theory and its application. Science Press, Beijing (in Chinese)
- Ou CB, Yu YN, Zhang YP, et al. (2005) Study on variable coefficient GAM model of settlement prediction. *Low Temp Archit Technol* 18: 76–78 (in Chinese)
- Qi L, Zhuang XJ, Chen SS (2004) Analysis of initial in-situ stress field using gray algebraic curve model. *Water Resour Hydropower Eng* 35:42–44 (in Chinese)
- Razani M, Yazdani-Chamzini A, Yakhchali SH, et al. (2013) A novel fuzzy inference system for predicting roof fall rate in underground coal mines. *Saf Sci* 55:26–33
- Saeedi G, Shahriar K, Rezaei B (2013) Estimating volume of roof fall in the face of longwall mining by using numerical methods. *Arch Min Sci* 58:767–778
- Satyanarayana I, Budi G, Deb D (2015) Strata behaviour during depillaring in blasting gallery panel by field instrumentation and numerical study. *Arab J Geosci* 8:6931–6947
- Tan YL, He KX, Ma ZS, et al. (2006) The telemetering prediction system concerning the separation of hard roof caving. *Chin J Rock Mech Eng* 25:1705–1709 (in Chinese)
- Tang JX, Deng YH, Tu XD, et al. (2010) Analysis of roof separation in gob-side entry retaining combined support with bolting wire mesh. *J China Coal Soc* 35:1827–1831 (in Chinese)
- Wang YY (2012) Method for data association of radar with ESM based on GAM. *Command Inf Syst Technol* 3:40–45 (in Chinese)
- Xie JL, Xu JL (2015) Ground penetrating radar-based experimental simulation and signal interpretation on roadway roof separation detection. *Arab J Geosci* 8:1273–1280
- Xu QY, Zhao YJ, Li YM (2015) Statistical analysis and precautions of coal mine accidents in China. *Coast Eng* 47:80–82 (in Chinese)
- Yan H, Zhang JX, Wang SG, et al. (2014) Simulation study on key influencing factors to the roof abscission of the roadway with extra-thick coal seam. *J Min Saf Eng* 31:681–686 (in Chinese)
- Zhang GH, Liang B, Zhang HW, et al. (2010) Analysis of the roof separation in mining roadway and technical parameters determination of bolt combined supporting. *J Chongqing Univ* 33:135–139 (in Chinese)
- Zhao ZG, Zhang YJ, Li C, et al. (2015) Monitoring of coal mine roadway roof separation based on fiber Bragg grating displacement sensors. *Int J Rock Mech Min Sci* 74:128–132